JOURNAL OF GEOPHYSICAL RESEARCH, VOL. 106, NO. D12, PAGES 12,437-12,448, JUNE 27, 2001

Momentum transfer over the coastal zone

Jielun Sun,[1,2] Douglas Vandemark,[3] Larry Mahrt,[4] Dean Vickers,[4] Timothy Crawford,[5] and Christoph Vogel[6]

Abstract. Spatial variations of surface stress over the coastal shoaling zone are studied offshore of Duck, North Carolina, by the LongEZ research aircraft, equipped to measure both atmospheric turbulence and oceanic waves. We find that the spatial variation of the friction velocity with offshore distance is much larger with offshore flow than with onshore flow. In general, the mean square slope of the short waves (wavelength shorter than 2 m) decreases with offshore distance, while the mean square slope of the long waves (wavelength longer than 2 m) increases with offshore distance. With onshore flow the friction velocity is strongly correlated with surface waves. In addition, the variation of the neutral drag coefficient is well correlated with the atmospheric bulk Richardson number. With offshore flow the observed momentum flux significantly decreases with offshore distance. Within the first few kilometer offshore, the relationship between the friction velocity and the mean square slope of the short waves and the relationship between the neutral drag coefficient and the atmospheric bulk Richardson number are obscured by the direct influence of the upstream land surface on the measured turbulence. These relationships for offshore flow agree well with those for onshore flow if the fetch is beyond the immediate influence of the land surface. The results in this study suggests that the effects of the strong turbulence advected from over the nearby land surface in offshore flow may lead to ambiguous physical interpretation of the correlation between the momentum flux and the wave state.

1. Introduction

Surface stress over the sea has been investigated over open water from ships and aircraft and over coastal water with research towers [*Geernaert and Plant*, 1990; *Weller et al.*, 1991; *Kraus and Businger*, 1994; *Mahrt et al.*, 1996]. Numerous researchers have found that the stress is greater over a young and developing wave field than over an older wave field [*Kitaigorodskii*, 1973; *Geernaert et al.*, 1987; *Donelan*, 1990; *Donelan et al.*, 1993]. Developing waves are commonly observed with atmospheric flow acceleration (changing wind direction or speed), and fetch-limited offshore flow [*Geernaert et al.*, 1987], while the older wave field is closer in equilibrium with the wind field. Young developing waves (small wave age) are dominated by the growth of high-frequency capillary waves and small gravity waves that ride on the top of long gravity waves, travel slower than the wind, and thus lead to high surface stress [*Donelan*, 1982; *Geernaert et al.*, 1986].

Fully developed waves (larger wave age) move with a phase speed close to the wind speed and are associated with relatively low surface stress. Analysis of RASEX (RisøAir-Sea Experiment) data indicated that most of the variation of the drag coefficient could be explained in terms of wave age although self-correlation through the friction velocity accounted for much of this explained variance, and the broadness of the wave spectra explained additional variance [*Vickers and Mahrt*, 1997a]. The influence of directional differences of the wind, wind stress, and surface waves on the open ocean has been studied by *Geernaert* [1988a], *Geernaert et al.* [1993], and *Rieder et al.* [1994].

Interactions between the stress and the sea surface immediately off coastlines are not fully understood [*Mahrt et al.*, 1996, 1998; *Mahrt*, 1999]. In the coastal zone, large stress is expected with shoaling processes and wave breaking as swell propagate into shallow water [*Smith*, 1980; *Freilich and Guza*, 1984]. Therefore spatial variations of turbulent fluxes over the coastal

[1]National Center for Atmospheric Research, Boulder, Colorado.

[2]Also at Program in Atmospheric and Oceanic Sciences, University of Colorado, Boulder, Colorado.

[3]NASA Goddard Space Flight Center, Wallops Island, Virginia.

[4]College of Oceanic and Atmospheric Sciences, Oregon State University, Corvallis.

[5]NOAA Field Research Division, Idaho Falls, Idaho.

[6]NOAA Atmospheric Turbulence and Diffusion Division, Oak Ridge, Tennessee.

Paper number 2000JD900696.
0148-0227/01/2000JD900696$09.00

zone are expected to be large [*Crawford et al.*, 1993; *Mahrt*, 1999].

For the first time, the spatial variation of the air-sea interaction in the shoaling zone is studied with both atmospheric and surface-wave observations on board the research aircraft, LongEZ. The observed atmospheric and oceanic data used in this study are described in section 2. Methods of data analysis are explained in section 3. The momentum transfer between the atmosphere and the sea surface is investigated for onshore and offshore flows in section 4. A summary of the study is given in section 5.

2. Observations

Two experiments were conducted off the coast of Duck, North Carolina, one from October 26 to November 12, 1997, and the other one from March 1 to 17, 1999. The LongEZ aircraft (Figure 1) was equipped to measure all three wind components, air temperature, and atmospheric pressure at 50 samples per second, and surface radiation temperature (Everest Interscience Inc., 4000.4GL infrared radiometer) at 1 sample per second [*Crescenti et al.*, 1999]. The high sampling rate and the fast-response instrumentation of the air-motion measurements enables us to calculate atmospheric turbulent fluxes using eddy-correlation methods. The aircraft typically flies at 55 ms^{-1} at 15 m above the sea surface.

Three laser altimeters (Riegl model LD90-3 VHS) were mounted in a triangle with triangle legs of 0.93 m, 0.94 m, and 0.94 m to simultaneously measure sea surface wave heights [*Vandemark et al.*, 2000]. The laser range accuracy and precision are better than 2 cm. The minimum surface wave length derived from the laser altimeters is about 2 m. A downward looking Ka-band continuous wave (CW) radar scatterometer was also on board, and its 1 m diameter field of view overlays the field of view of the three laser altimeters [*Vandemark et al.*, 2000]. In addition to the onaboard downward looking scatterometer and the three laser altimeters, a Datawell Directional Waverider buoy, moored at about 20 m depth and 5 km offshore, was operated by Thomas Herbers's group at the Naval Postgraduate School during the 1997 experiment.

There were 16 aircraft flights conducted in the 2 week experiment in November, 1997, and 23 aircraft flights in the 3 week experiment in March 1999. Repeated runs for each flight track were designed to ensure adequate flux sampling. Two main flight patterns were flown to study spatial variations of atmospheric turbulence and surface waves as functions of offshore distance: one consists of tracks parallel to the coastline at various offshore distances; and one consists of many repeated runs along a track perpendicular to the coastline (Figure 2). For the parallel track flight, there are typically two to four passes along each track. For the perpendicular track flight there are typically eight passes. During both experiments the tracks parallel to the coastline are about 20 km long. The track perpendicular to the coastline is about 10 km long and is extended to 90 km offshore for some flights. In this study we mainly focus on flights with both the atmospheric turbulence and the wave data available. On the basis of these criteria, four parallel flights (Flights 5, 12, 14, and 15) and two perpendicular flights (Flights 3 and 16) from the 1997 experiment and three parallel flights (Flights 5, 9, and 10) from the 1999 experiment are selected (Table 1). Among these nine flights, the radar data are available for all the flights except Flight 12 from the 1997 experiment. The wind was onshore for Flights 14 and 15 of the 1997 experiment, offshore for Flights 3, 5, 12 of the 1997 experiment, and Flights 5 and 9 of the 1999 experiment, and almost parallel to the coastline for Flights 16 of the 1997 experiment and Flight 10 of the 1999 experiment (Table 1).

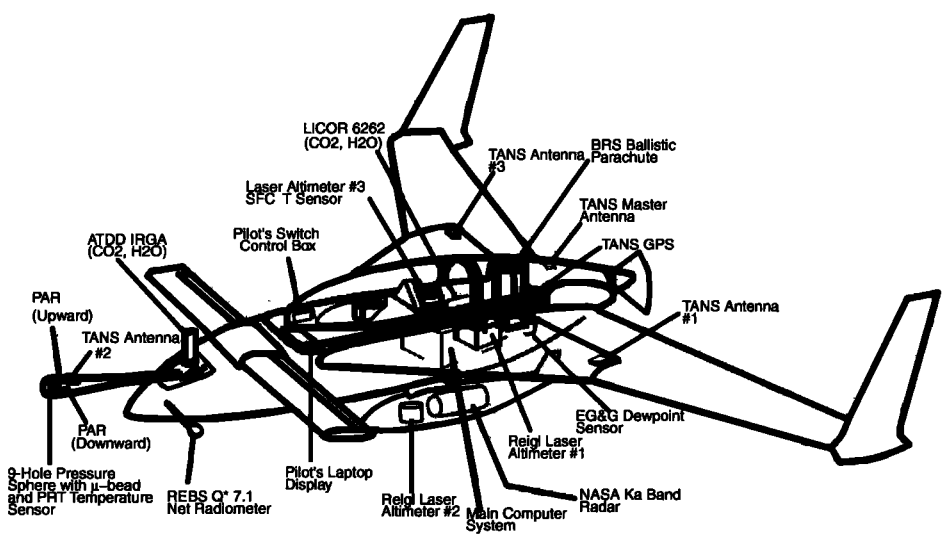

Figure 1. Schematic diagram of the equipment on the NOAA LongEZ.

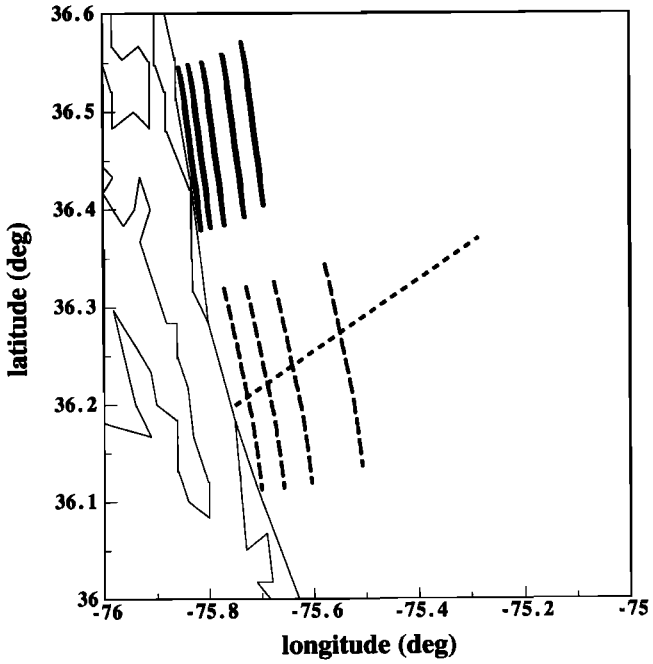

Figure 2. Schematic diagram of flight tracks. The solid lines are the parallel tracks in the 1999 experiment. The dashed lines are the parallel tracks and the perpendicular track in the 1997 experiment.

3. Data Processing

The aircraft position and velocity are obtained by combining differential GPS (global positioning system) with the information from the accelerometers, recorded at 10 samples per second and 50 samples per second, respectively. The aircraft platform attitude is obtained by combining TANS (Trimble Advanced Navigation System) GPS attitude, recorded at 10 samples per second, with the information from the accelerometers [*Crawford and Dobosy*, 1992].

All the aircraft data used for the analysis in this paper were quality-controlled following *Vickers and Mahrt* [1997b]. After eliminating records with apparent instrumentation problems, the turbulent fluxes are calculated by averaging products of the perturbations from nonoverlapping windows of 1 km width. The qualitative results of this study, such as the general character of the spatial variation of turbulent fluxes, were not sensitive to the averaging window size. Assuming spatial homogeneity along each flight track, the random flux error (f_{err}) for the momentum transfer is normally less than 8% for the repeated flight tracks parallel to the coastline. Here the random flux error f_{err} is calculated as

$$f_{err} = \frac{\sigma_f}{\sqrt{N}}, \tag{1}$$

where σ_f is the standard deviation of the flux for a given flight track, and N is the total number of 1 km flux values. For the parallel flight track, N is typically between 40 and 80 for each flight track.

The nadir-looking radar backscatter is measured as the normalized radar cross section (NRCS), which is inversely correlated with the mean square slope (mss) of these surface waves [*Barrick*, 1974; *Vandemark et al.*, 1997],

$$\mathrm{mss} = C \times 10^{(-\mathrm{NRCS}/10)}, \tag{2}$$

where the Fresnel reflection coefficient C for the *Ka*-band (36 GHz) radar is 0.52. At a 15 m flight level, the instantaneous backscatter encompasses surface waves with horizontal length scales of 1 m down to scales of the order of the 8 mm radar radiation wavelength; that is, the instantaneous radar backscatter signal strength depends on surface waves with wavelengths between 1 m and 25 cm. The total mean square slope estimate is derived from the ensemble of the NRCS over the two-scale process of sweeping this 1 m field of view along varying underlying waves as the aircraft flies over a given flight segment. Theoretical prediction and measurements indicate that surface wind stress and nadir-looking radar backscatter are related to the integrated wave slope [*Brown*, 1979; *Kitaigorodskii*, 1973], particularly in the capillary-gravity-wave range [*Wu*, 1972]. A typical averaging segment is 3 km, and the computed random error for a given NRCS estimate is of the order of 2% [*Vandemark et al.*, 2000].

The mean square slope of the surface waves for wavelengths longer than 2 m can be calculated from the three simultaneous laser altimeter measurements corrected for the aircraft motion [*Vandemark et al.*, 2000].

Table 1. Flight Information

Case	Flight	Date	LT	Radar /Laser	Flow Versus Coast	Flight Track	Wind Direction (deg)	Wind Speed (m/s)
1	F3	Nov. 2, 1997	1153	yes	offshore	perpendicular	233.8	7.8
2	F5	Nov. 3, 1997	1326	yes	offshore	parallel	195.6	7.0
3	F12	Nov. 9, 1997	1301	no	offshore	parallel	286.6	8.2
4	F14	Nov. 10, 1997	1119	yes	onshore	parallel	32.2	3.6
5	F15	Nov. 10, 1997	1347	yes	onshore	parallel	73.8	2.6
6	F16	Nov. 11, 1997	0734	yes	parallel	perpendicular	356.3	5.8
7	F5	Mar. 4, 1999	1052	yes	offshore	parallel	272.4	11.2
8	F9	Mar. 6, 1999	1006	yes	offshore	parallel	189.5	7.7
9	F10	Mar. 7, 1999	1028	yes	parallel	parallel	339.4	13.3

For simultaneous measurements from three laser altimeters the unit vector normal to the wave surface measured by the three lasers, $\vec{S}$, is

$$\vec{S} = \frac{(\vec{L}_3 - \vec{L}_2) \times (\vec{L}_2 - \vec{L}_1)}{|\vec{L}_3 - \vec{L}_2| \cdot |\vec{L}_2 - \vec{L}_1|}. \quad (3)$$

Here $\vec{L}_1 = (x_1, y_1, z_1)$, $\vec{L}_2 = (x_2, y_2, z_2)$, and $\vec{L}_3 = (x_3, y_3, z_3)$ represent the locations of the intersections between the three laser beams and the sea surface. The distances, z_1, z_2, and z_3, are measured from the three laser altimeters with the aircraft motion removed, and the coordinates x_i and y_i $(i = 1, 2, 3)$ are the location of the three lasers relative to the aircraft gravity center on the horizontal aircraft plane . The sea surface slope s is then

$$s = \tan(\theta), \quad (4)$$

where

$$\cos(\theta) = \vec{S} \cdot \vec{k}. \quad (5)$$

Here $\vec{k}$ is the upward unit vector, and θ is the angle between the wave surface and the flat sea surface.

The total mean square slope for the surface waves measured using three lasers, mss_l, can be readily estimated as

$$\text{mss}_l = \frac{1}{M} \sum_{i=1}^{M} s_i^2, \quad (6)$$

where s_i is the slope s at each time i, and M is the total number of the laser range measurements used for estimating mss_l. In this study, M is 3000 for a 3 km segment. Several calibration flights with substantial aircraft roll and pitch maneuvers were performed over smooth water on the inland sound to asses the fidelity of the aircraft motion removal on the derived sea surface elevation and wave slope data. For these cases the mss_l value was typically less than 0.002 with along-track variations of less than 10%. On the basis of these tests we conservatively estimate the maximum relative error for open-ocean mss_l to be 5%.

The mean square slope of short waves (mss_s) for wavelengths shorter than 2 m can be estimated by combining the mean square slope of the integrated surface waves from the radar scatterometer (mss) for wavelengths longer than 2.5 cm and the mean square slope of the surface waves from the laser altimeters (mss_l) for the wavelengths longer than 2 m,

$$\text{mss}_s \approx \text{mss} - \text{mss}_l; \quad (7)$$

that is, the mean square slope of the short waves is estimated as the difference between the mean square slope of "total" wave field estimated from the radar scatterometer and the mean square slope of the long waves estimated from the laser altimeters. Therefore mss_s is derived from the measurements of two different instruments.

Assuming the homogeneity of each flight track, all the observed variables, including the turbulent fluxes and the mean square slope of the surface waves: mss_s, mss_l, and mss are averaged from repeated 20 km long passes over each flight track for the tracks parallel to the coastline to study the spatial variation of these variables as a function of offshore distance. The fluxes and the mean square slope of the surface waves along the flight tracks perpendicular to the coastline are fitted as a function of offshore distance based on repeated passes.

One-dimensional wave height spectra for those waves propagating along the flight direction can be derived from the spatial wave elevation series collected from any of the three laser altimeters aboard the LongEZ after adjusting for aircraft motion. For waves traveling perpendicular to the aircraft heading, some a priori knowledge of their direction is required when using measurements from only one laser altimeter. The wave measurement from the altimeter is analogous to wave measurements from wave rider buoys, except wave rider buoys measure wave heights as functions of time, while laser altimeters measure wave heights as functions of horizontal distance.

The atmospheric stability in this study is expressed in terms of the bulk Richardson number (R_i),

$$R_i = -\frac{g\ \Delta\theta\ z}{\theta_0\ U^2}, \quad (8)$$

where

$$\Delta\theta = T_s - T_a. \quad (9)$$

In equations (8) and (9), g is the gravity constant, z is the observation height, θ_0 is the reference potential temperature, set to be 285.15 K, U is the wind speed, and T_s and T_a are the sea surface skin temperature measured by the infrared radiometer and the air temperature measured from the LongEZ, respectively.

4. Spatial Variations of Stress in the Shoaling Zone

Surface stress ($\vec{\tau}$) between the atmosphere and the sea surface over open water can be estimated as

$$\vec{\tau} = \rho(\overline{w'u'}\ \vec{i} + \overline{w'v'}\ \vec{j}), \quad (10)$$

where ρ is the air density; u', v', and w' are the wind speed fluctuations in the north-south $\vec{i}$, east-west, $\vec{j}$, and vertical, $\vec{k}$, directions, respectively. In this study, the mean value is defined as an unweighted window average over 1 km. The strength of the stress will be expressed in terms of the friction velocity (u_*), defined as

$$\tau = \rho u_*^2. \quad (11)$$

On the basis of Monin-Obukhov similarity theory the friction velocity depends on wind speed, atmospheric stability, and sea surface roughness; that is,

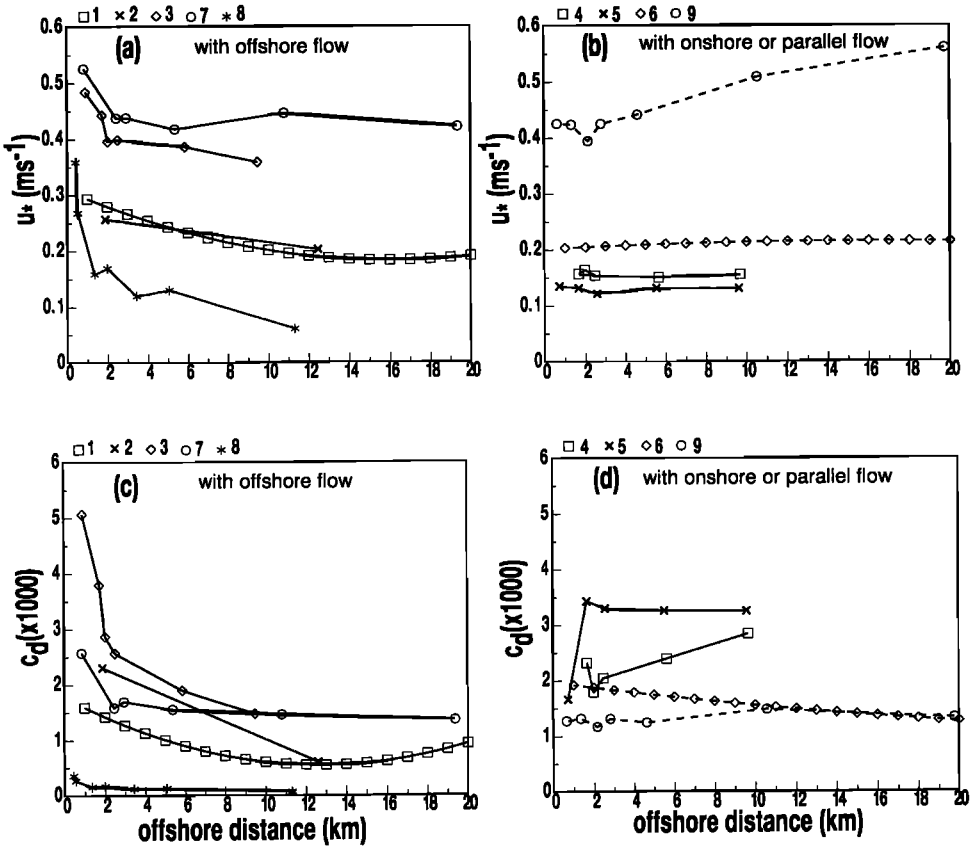

Figure 3. Friction velocity (u_*) (a, b) and drag coefficient (C_d) (c, d) as functions of offshore distance for onshore flow (b, d), and offshore flow (a, c) cases. Each individual symbol represents composited results from one flight. The numbers at the top of each panel represent the case number listed in Table 1. The dashed lines in Figures 3b and 3d represent the cases where the flow is almost parallel to the coast.

$$u_* = C_d^{1/2} U, \tag{12}$$

where

$$C_d^{1/2} = \frac{\kappa}{\ln(z/z_0) - \Psi_m(z/L)}. \tag{13}$$

Here C_d is the drag coefficient, U is the mean wind speed, z_0 is the aerodynamic roughness length, κ is the von Karman constant, and Ψ_m is the stability function for momentum expressed in terms of z/L, where $L = -\bar{\theta}_v u_*^3/(\kappa g \overline{w'\theta_v'}|_s)$ is the Obukhov length, and θ_v and $\overline{w'\theta_v'}|_s$ are the virtual potential temperature and the buoyancy flux at the surface, respectively. In this study, the *Paulson* [1970] and *Dyer* [1974] stability functions are used for unstable and stable regimes, respectively. The ocean current is assumed to be much smaller than the wind speed in equation (12). Removing the stability influence in equation (13), the neutral drag coefficient can be expressed as

$$C_{d0}^{1/2} = \frac{\kappa}{\ln(z/z_0)}. \tag{14}$$

If z is constant, the neutral drag coefficient is monotonically related to the aerodynamic roughness length z_0, which is related to the physical roughness of the underlying surface if the stress is generated by the interaction between the airflow and the underlying wave surface. Using the aircraft observational data, the neutral drag coefficient can be calculated using equations (10)-(14).

4.1. Spatial Variation of Stress As a Function of Offshore Distance

On the basis of the LongEZ data described in section 2 the surface friction velocity significantly decreases with offshore distance within the first several kilometers off the coast in offshore flow (Figure 3a), while the corresponding spatial variation of the friction velocity for onshore flow is small (Figure 3b). The difference in the spatial variation of the surface stress between the onshore and the offshore flow cases is also clearly demonstrated in terms of the drag coefficient (Figure 3c and 3d), in which case the dependence of the stress on the wind speed has been removed (equation (13)). The drag coefficient systematically decreases with offshore distance in the offshore flow cases but not in the onshore flow cases.

For scalar quantities the rapid change of the observed flux with fetch, immediately downstream from

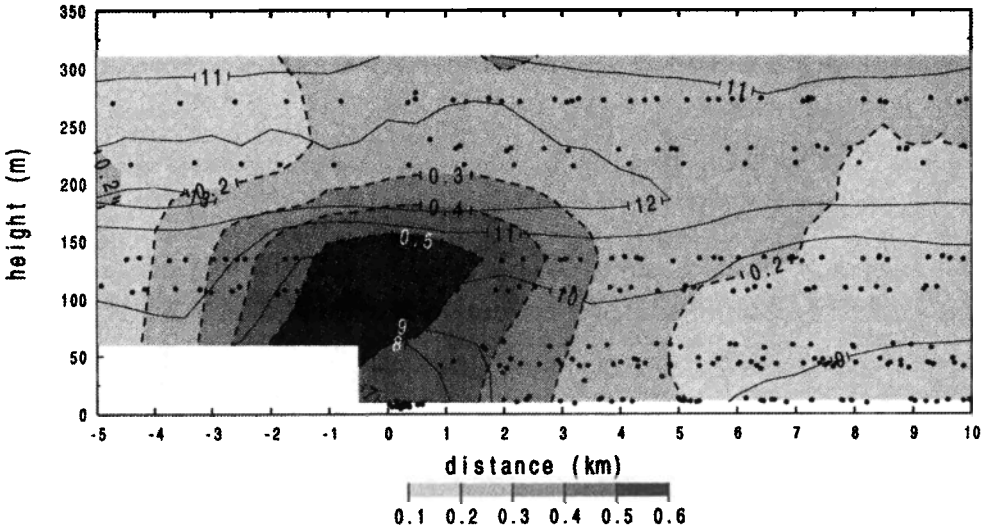

Figure 4. Vertical cross section of the friction velocity (shaded with dashed contours) and the wind speed (solid contours) for November 14, 1999. Here zero distance represents the Atlantic coastline of Outer Banks. The Outer Banks are about 4.2 km wide in this cross section. The negative distance represents the distance west of the Atlantic coastline of the Outer Banks. The plot is based on aircraft measurements of the friction velocity calculated from 1 km segments. The 1 km segments used for this plot are indicated by the dots. The wind was offshore from the southwest. The technique for construction of the distance-height crosssection is described by *Vickers et al.* [2001].

the coast, can be viewed in terms of footprint theory. For momentum, stress and turbulence energy the footprint theory is not strictly valid because footprint theory is formally based on the advective-diffusion equation, and the role of pressure fluctuations and viscous decay are not included. We will continue to use the term "footprint" in a more descriptive context as the upstream surface region, which contributes to the momentum flux at the observation level.

With this concept the flux measured at the aircraft level contains contributions from both the sea and the upstream land surface. The contribution of the upstream land surface decreases with fetch. According to *Horst and Weil* [1994], 90% of the turbulent scalar flux measured at the height of 10 m typically originates from a footprint extending 1-2 km upstream although the footprint varies with atmospheric stability and wind speed. The vertical cross section of the momentum transfer extended to the inland sound (Figure 4) indeed shows that the rough unstable land surface between the inland sound, and the Atlantic Ocean plays an important role on the observed momentum transfer immediately off the Atlantic coastline. Therefore the true interaction between the turbulent air and the sea surface is obscured by the direct influence of the upstream land surface on the measured stress.

4.2. Spatial Variation of Surface Waves

As momentum is transferred from the atmospheric flow to the ocean by the atmospheric turbulence, surface wind waves are generated. In general, the mean square slope of the short waves (mss_s) decreases with offshore distance for both onshore and offshore flow cases. The mean square slope of the long waves (mss_l) increases with offshore distance when the wind is offshore (Figure 5).

When the flow is onshore, mss_l generally increases with offshore distance, except when the offshore distance is less than 2 km, where mss_l increases toward the coast apparently due to shoaling (Figure 5e). Such shoaling increases mss_s as well as mss_l. A similar shoaling effect was also observed by *Anctil and Donelan* [1996]. The exception for case 9 in Figure 5d is most likely due to the increase of the wind speed with the offshore distance (section 4.3).

An example of one-dimensional spectra on November 1997 (case 1 in Table 1) when the LongEZ flew perpendicular to the coastline is analyzed in this study to assess the impact of the longer waves (swell and wind-driven surface waves) on the mean square slope of surface waves in offshore flow. For the present example we broke the flight data into 2 km data segments along the flight track. Each 2 km segment contains approximately 2000 data points. A continuous Morlet wavelet transform [*Torrence and Compo*, 1998] was performed on each data segment to produce a wave-height density spectrum at each offshore distance.

On the basis of the nearby wave rider buoy data, the wind-driven sea surface waves propagated toward the northeast, and the swell traveled to the northwest (300°) with a period of 9 s. The existence of swell and wind-driven waves are evident in Figure 6a, where the

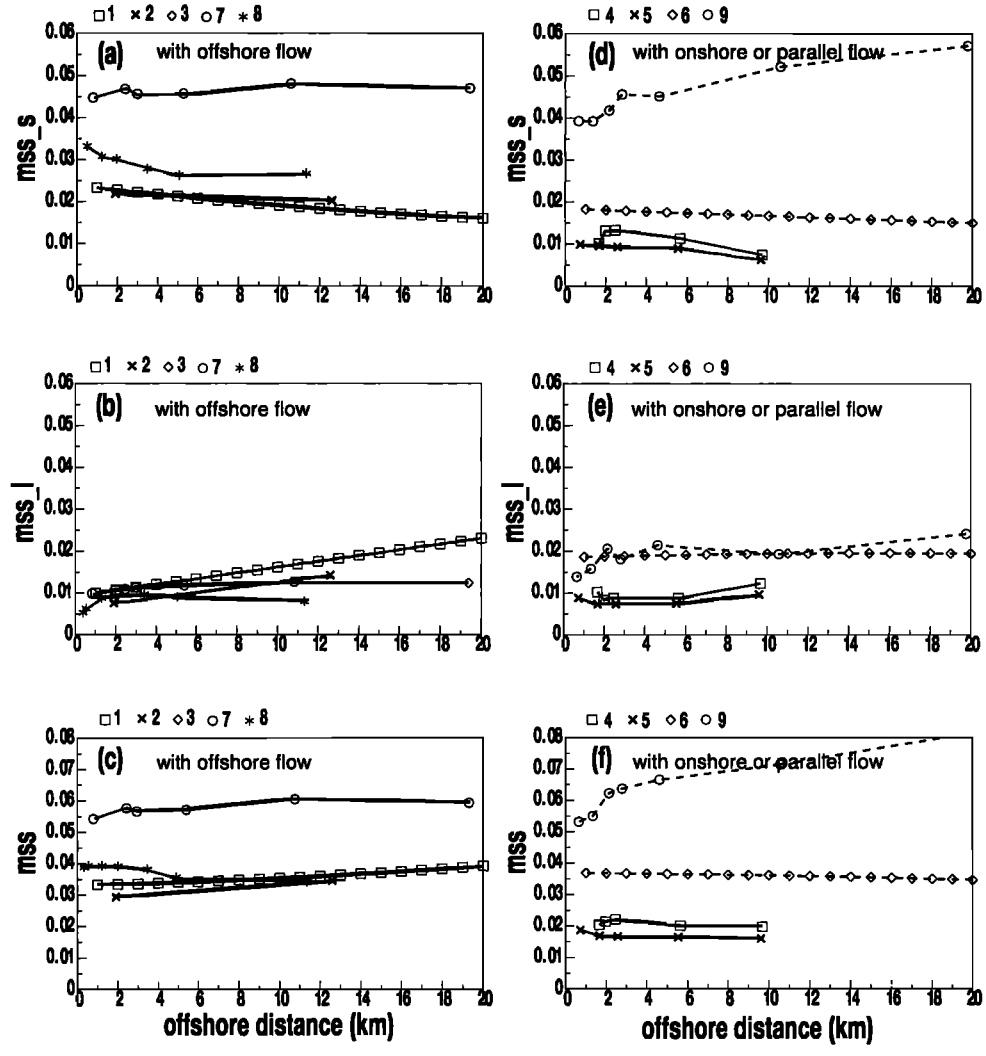

Figure 5. Mean square slopes of short surface waves (less than 2 m) (a, d), long surface waves (longer than 2 m) (b, e), and the sum of the short and long surface waves (c, f) observed by the radar and the laser altimeters as functions of the offshore distance for the onshore (d, e, f) and offshore (a, b, c) flows. The dashed lines represent the case in which the flow is almost parallel to the coastline.

derived swell wave number accords with the 9 s period swell measured by the nearby buoy. The difference between the wave spectra at 2 km and 10 km offshore in Figure 6a shows that the peak wave number of the wind-driven waves decreases with increasing offshore distance, and the amplitude of the wind-driven waves increases with increasing offshore distance as the aircraft flew nearly along the direction of the wind-driven wave propagation (Figure 6b). This spatial variation of the wind-driven surface wave is consistent with the observations from *Hasselmann et al.* [1973]. In comparison, both the wave number and the energy of the swell remained invariant (Figure 6a and 6b). Therefore the increase of the significant wave height with offshore distance is due to the increased energy of the growing wind-driven surface waves in the presence of the incoming swell (Figure 6c). Here the significant wave height is calculated as 4 times the root-mean-square wave height. The invariant swell height of about 1 m can be estimated from Figure 6c near the coastline, where the wind-driven surface wave height is negligible. These results imply that the increase of mss_l with offshore distance is closely related to the increasing wind-driven wave energy with offshore distance and the shift of the wind-driven waves to larger wavelengths.

4.3. Relationship Between Wind Stress and Sea Surface Roughness

For the offshore flow case, the large mean square slope of the short waves close to the coast is related to the young waves generated by the turbulent air as the sea surface responds to the atmospheric momentum flux. As these waves propagate offshore, the new wind-driven short waves transfer the energy to longer waves due to wave-wave interaction, as inferred in section 4.2. There is no sharp decrease of the mean square slope of short

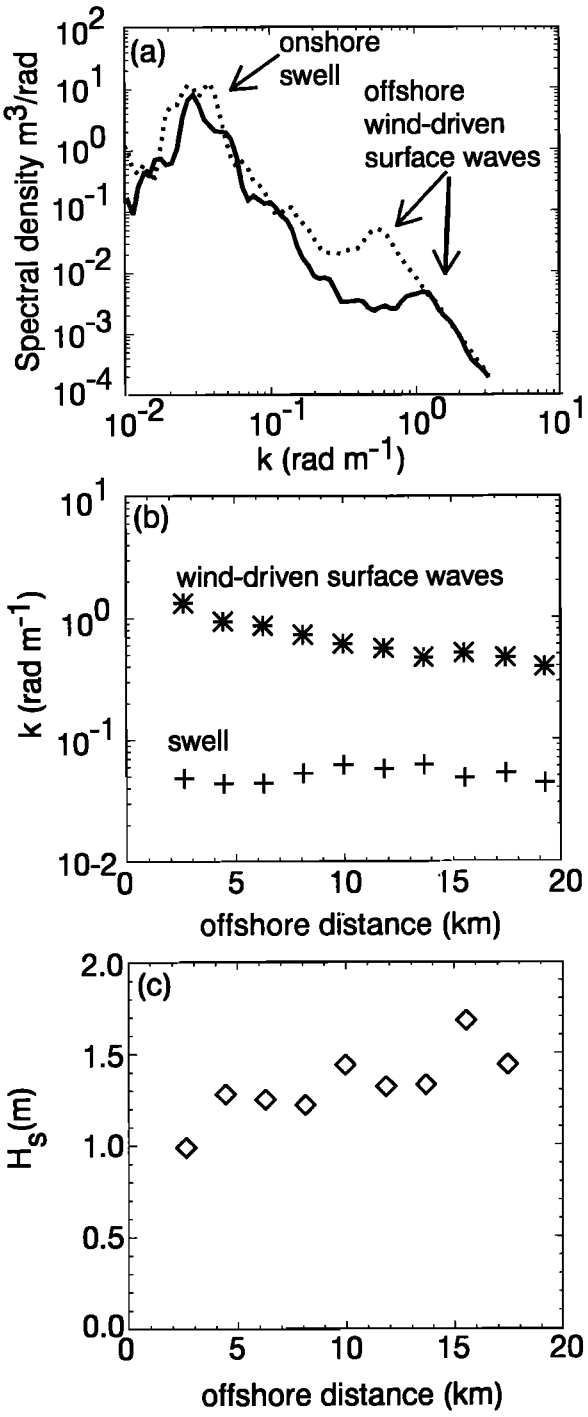

Figure 6. Wave analysis from a laser altimeter. (a) Wave height density spectra as functions of wave number at 2 km (solid line) and 10 km (dotted line) offshore. (b) The spectral peak wave numbers of the incoming swell (pluses) and the wind-driven waves (asterisks) as functions of offshore distance. Here the peak wave number of the swell is adjusted to account for the 60° angle between the swell propagation direction and the aircraft heading. (c) Significant wave heights as functions of offshore distances.

and long waves (Figure 5) for the first several kilometers offshore, in contrast to the sharp decrease of the friction velocity with the offshore flow (Figure 3). Since the observed momentum flux includes the influence of the upstream land, while the mean square slope of waves represents the sea surface state right under the observational point, the footprint of these two quantities is mismatched. The mismatch of the footprint is not very important if the spatial variation of the surface does not vary dramatically, as in onshore flow. *Nordeng* [1991] indicates that surface waves do not generate significant stress when the waves are very young, implying that the large momentum flux observed right off the coastline cannot be attributed completely to young waves. Because the footprint of the momentum flux increases with increasing observation height, the downward momentum flux at higher levels includes the land surface and is therefore larger compared to the momentum flux near the surface (Figure 4). This resulting vertical convergence of the downward momentum flux accelerates the offshore flow (Figure 7), which is also observed by *Smedman et al.* [1995].

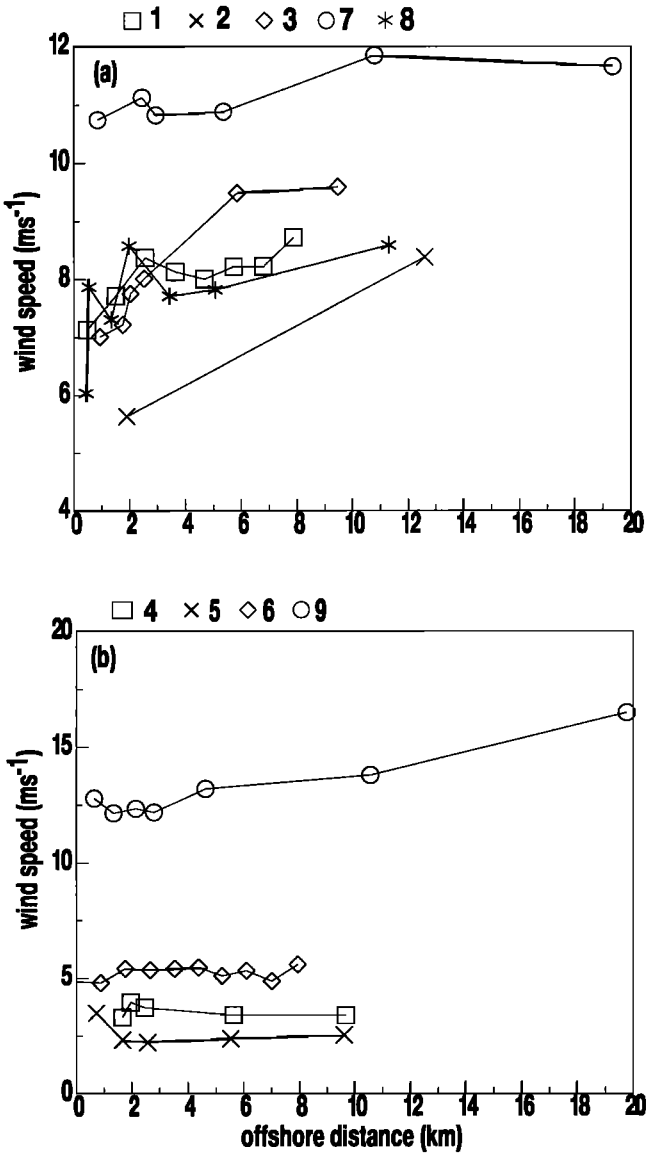

Figure 7. Wind speed as a function of offshore distance for offshore flow (a) and onshore/parallel flow (b).

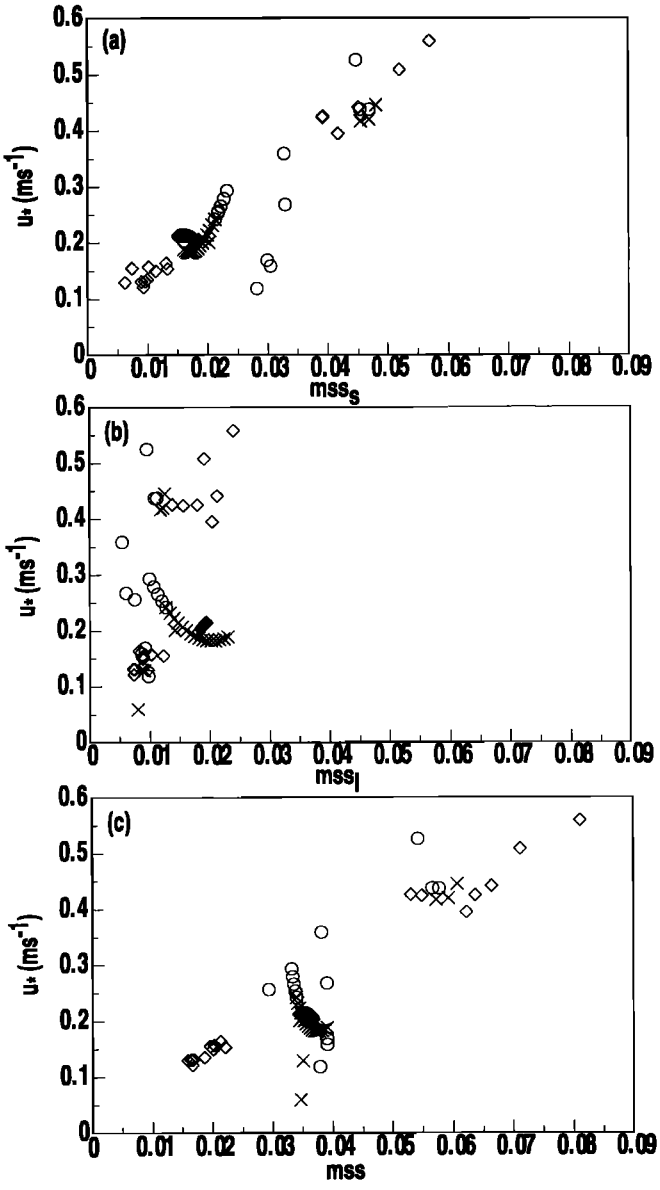

Figure 8. Relationship between the friction velocity and the mean square slope of (a) short surface waves (less than 2 m), (b) long (longer than 2 m) surface waves, and (c) the sum of the short and long surface waves observed by the radar and the laser altimeters for the onshore (diamonds) and offshore (circles and crosses are for off-distance less and greater than 5 km, respectively) flows.

With onshore flow the friction velocity and the mean square slope of the short waves are closely correlated (Figure 8), consistent with previous observations [*Cox and Munk*, 1954; *Brown et al.* 1981; *Vandemark et al.*, 1997, 1999]. For offshore flow the friction velocity is not well correlated with the mean square slope of the short waves within 5 km of the coast. Farther offshore, the relationship between the friction velocity and the mean square slope of the short waves agrees reasonably well with the relationship for the onshore flow (Figure 8).

For offshore flow and beyond 5 km offshore, the correlation between the friction velocity and mss_l is not so good as the correlation between the friction velocity and the mss_s and not so good as the correlation between the friction velocity and the mss_l for the onshore flow case. *Vickers and Mahrt* [1997a] find that the wave spectra are broader for the offshore flow than for the onshore flow. As discussed in section 4.2, our example case shows that the energy of the waves increases with offshore distance, and the peak of the wave spectra progressively shifts toward lower frequencies as the fetch increases. These long waves may result from interactions between waves that are generated upstream. These long waves can travel fast and may not be fully coupled with the surface stress. In contrast, the close correlation between the friction velocity and the mss_s in offshore flow for more than 5 km from shore indicates that the short waves are in equilibrium with the surface wind forcing.

4.4. Influence of the Atmospheric Stability on the Wind Stress

The surface roughness of the ocean ripples (mainly the capillary waves) is found to increase with the atmospheric instability [*Keller et al.*, 1985; *Hwang and Shemdin*, 1988; *Wu*, 1991]. The enhanced turbulence under unstable conditions leads to greater sea surface ripples and sea surface roughness, in contrast to stability-independent roughness lengths over land surfaces [*Sun*, 1999].

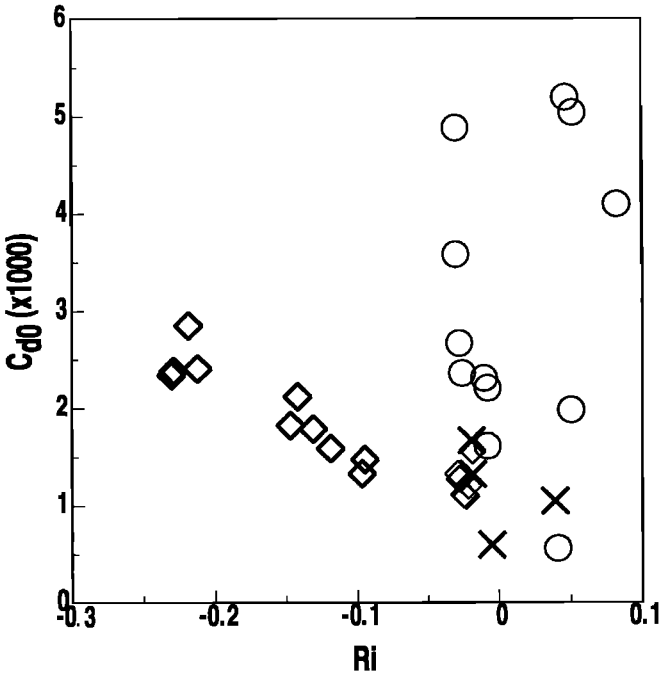

Figure 9. Neutral drag coefficient (C_{d0}) as a function of the bulk Richardson number (R_i) for both onshore (diamonds) and offshore flows (circles). The crosses represent the situation where the wind is offshore, but the offshore distance is larger than 5 km.

Figure 9 shows that the neutral drag coefficient does increase with atmospheric instability systematically for the onshore case where the downward momentum transfer is completely associated with the interaction between the atmosphere and the oceanic waves. This stability dependence of the neutral drag coefficient was also observed by *Plant et al.* [1998]. They suggested that the surface roughness increases in unstable conditions where the downward transfer of momentum to the wave surface is more efficient.

For offshore flow the neutral drag coefficient close to the coast is inevitably affected by the upstream land surface since the fluxes at the aircraft level are affected by the upstream land surface. However, the bulk Richardson number is the bulk parameter based on the mean variables over the sea surface alone. Therefore the neutral drag coefficient near the coast in offshore flow is not well correlated with the bulk Richardson number. As the footprint of the momentum flux becomes occupied completely by the sea surface when the offshore distance is larger than 5 km, the correlation between the neutral drag coefficient and the bulk Richardson number agrees reasonably well with the correlation for the onshore flow cases (Figure 9). The relationship between the neutral drag coefficient and the atmospheric stability for the onshore flow and longer fetch offshore flow implies that the spatial variation of the atmospheric stability may also play an important role in the spatial variation of the sea surface roughness.

4.5. Discussion

Geernaert [1988b] summarized seven regression formulas for the neutral drag coefficient as a function of wind speed. He found that the neutral drag coefficient was much larger over shallow water than over open water. The large neutral drag coefficient over shallow water cannot be explained entirely by the fetch-dependent sea state, therefore shoaling effects were suggested as a possible explanation. As indicated in this study, the large momentum flux observed in the coastal area with offshore flow is very likely influenced by the advection of the large momentum flux from the land surface. Therefore the advection from the land surface may explain part of the discrepancy between the observed and the modeled, wave-dependent neutral drag coefficient in the *Geernaert* [1988b] work.

Traditionally, the drag coefficient in the coastal zone is studied in terms of fetch and wave age. The wave age is designed to characterize the movement of the wind relative to surface wave motion, and in one version of the wave age is defined as the ratio of the phase speed of the most significant wave relative to the wind speed. When the wave phase speed is much slower than the wind speed (small wave age), strong atmospheric flow relative to the waves induces large drag at the sea surface. When the wave phase speed is comparable to the wind speed, the surface stress between the atmospheric motion and the moving surface waves is small [*Al-Zanaidi and Hui*, 1984]. However, the interaction between the wind and the surface waves other than the significant wave may also contribute to the surface stress when the wind-wave spectra have a wide band structure, especially when the wind generates waves on the top of the existing long waves [*Donelan et al.*, 1993; *Vickers and Mahrt*, 1999].

Alternatively, the wave age is computed as the ratio between the phase speed of the significant wave and the friction velocity [*Geernaert et al.*, 1987; *Donelan et al.*, 1993] with the implied assumption that the footprint of the turbulent fluxes is completely over the sea surface. As demonstrated in this study, the stress over the coastal water can be influenced by the strong turbulence advected from land. The large momentum flux with the offshore flow would lead to a small value of the wave age (defined with the friction velocity instead of wind speed). The wave age calculated using the observed friction velocity close to the coast would not represent the true wave state until farther offshore when the measured stress is influenced only by the sea surface.

Fetch-dependent studies of the momentum transfer in the literature may have unknowingly captured the spatial variation of the footprint of the observed flux over the land surface. Using the footprint theory as guidance, the measured flux downstream from the land surface not only depends on the distance from the coast but also on the measurement height and upstream spatial variation of the atmospheric stability.

5. Summary

The spatial variation of the interaction between the atmosphere and the sea surface in the coastal zone is studied using simultaneous measurements of the atmospheric turbulence and the sea surface from the LongEZ research aircraft. In the coastal zone the spatial variation of the surface stress and the correlation between the surface stress and the sea surface roughness are distinctly different between the onshore and the offshore flows.

For onshore-flow the friction velocity is well correlated with the mean square slope of short surface waves with wavelengths shorter than 2 m, and with the mean square slope of long surface waves with wavelengths larger than 2 m. The mean square slopes of the short and long surface waves are derived from simultaneous measurements from the downward looking *Ka*-band radar scatterometer and the three laser altimeters onboard the aircraft. The neutral drag coefficient is well correlated with the atmospheric bulk Richardson number, confirming expected interactions between the sea surface waves and the turbulent air fluctuations.

However, for the offshore flow cases, the stress decreases rapidly with offshore distance for the first several kilometers. This sharp decrease in the momentum flux is most likely due to the decreasing influence of the

upstream land surface within the footprint of the flux measurement as the offshore distance increases. As a result of the influence of the upstream land surface, the neutral drag coefficient is not correlated with the atmospheric bulk Richardson number within the first 5 km off the coast. For offshore distances larger than 5 km the correlation between the neutral drag coefficient and the atmospheric bulk Richardson number agrees with the correlation for onshore flow, and the correlation between the friction velocity and the mean square slope of the short waves is also consistent with that for onshore flow.

With offshore flow the mean square slope of the short waves generally decreases with offshore distance and the mean square slope of the long waves generally increases with offshore distance. The spatial variation of the mean square slopes of the short and long waves are apparently due to the energy transfer from wind-driven young short waves to long waves through wave-wave interactions. With onshore flow the spatial variation of the mean square slope of both short and long waves is similar to the offshore flow case, except within 2 km offshore, the mean square slope of the long waves seems to increase slightly toward the coastline apparently due to shoaling.

The dependence of the neutral drag coefficient on the bulk Richardson number probably results from a relationship between the surface roughness and stability and the influence of advection of turbulence from the upstream land surface. This study demonstrates the complexity of air-sea interaction in the coastal zone, and the importance of simultaneous observations of atmospheric conditions and sea state. With the influence of the turbulence from the land surface, the measured momentum flux does not completely reflect the air-sea interaction. The wave age calculated using the observed momentum flux may not represent the true influence of wave state. The interaction between the momentum flux and the variation of the surface waves for the offshore case needs to be further studied with detailed wave spectra.

Acknowledgments. The comments of Bill Plant, Sean Burns, and two anonymous reviewers are greatly appreciated. We gratefully acknowledge Edward Dumas for collecting and processing the LongEZ aircraft data. The waverider buoy data were collected by T.H.C. Herbers with funding from the Office of Naval Research Coastal Dynamics Program. We are also thankful to the support from the Field Research Facility of the US Army Corps of Engineers at Duck, North Carolina. This work is supported by the Office of Naval Research. Jielun Sun is supported by grant N00014-97-1-0245, Douglas Vandemark is supported by grant N0001497F0179, Larry Mahrt and Dean Vickers are supported by grant N00014-97-1-0279, and Timothy Crawford and Christoph Vogel are supported by grant N00014-97-F-0123. The National Center for Atmospheric Research is sponsored by the National Science Foundation.

References

Al-Zanaidi, M. A., and W. H. Hui, Turbulent air flow over water waves: A numerical study, *J. Fluid Mech., 148*, 225-246, 1984.

Anctil, F., M. A. Donelan, Air-water momentum flux observations over shoaling waves, *J. Phys. Oceanogr., 26*, 1344-1353, 1996.

Barrick, D. E., Wind dependence of quasi-specular microwave sea scatter, *IEEE Trans. Antennas Propag., 22*, 135-136, 1974.

Brown, G. S., Estimation of surface wind speeds using satellite-borne radar measurements at normal incidence, *J. Geophys. Res., 84*, 3974-3978, 1979.

Brown, G. S., H. R. Stanley, and N. A. Roy, The wind-speed measurement capability of spaceborne radar altimeters, *IEEE J. Oceanic Eng., 6*, 59-63, 1981.

Cox, C., and W. Munk, Statistics of the sea surface derived from sun glitter, *J. Mar. Res., 13*, 198-227, 1954.

Crawford, T. L., and R. J. Dobosy, A sensitive fast-response probe to measure turbulence and heat flux from any airplane, *Boundary Layer Meteorol., 59*, 257-278, 1992.

Crawford, T. L., R. T. McMillen, T. P. Meyers, and B. B. Hicks, Spatial and temporal variability of heat, water vapor, and carbon dioxide, and momentum air-sea exchange in a coastal environment, *J. Geophys. Res., 98*, 12,869-12,880, 1993.

Crescenti, G. H., T. L. Crawford, and E. J.Dumas, Data report: LongEZ(N3R) participation in the 1999 Shoaling Waves Experiment (SHOWEX) spring pilot study, *NOAA Tech. Memo. ERL ARL-232*, Natl. Oceanic and Atmos. Admin., Washington, D. C., 1999.

Donelan, M. A., The dependence of the aerodynamic drag coefficient on wave parameters, In *First International Conference on Meteorological and Air/Sea Interaction of the coastal Zone*, pp. 381-387, Am. Meteorol. Soc., Boston, Mass., 1982.

Donelan, M. A., Air-sea interaction. in *Ocean Engineering Science*, edited by B. LeMehaute and D. M. Hanes, pp. 239-291, John Wiley, New York, 1990.

Donelan, M. A., F. W. Dobson, S. D. Smith, and R. J. Anderson, On the dependence of sea surface roughness on wave development, *J. Phys. Oceanogr., 23*, 2143-2149, 1993.

Dyer, A. J., A review of flux profile relationships, *Boundary Layer Meteorol., 7*, 363-372, 1974.

Freilich, M. H. R., and R. T. Guza, Nonlinear effects of shoaling surface gravity waves, *Philos. Trans. R. Soc. London, Ser. A, 311*, 1-41, 1984.

Geernaert, G. L., Measurements of the angle between the wind vector and wind stress vector in the surface layer over the North Sea, *J. Geophys. Res., 93*, 8215-8220, 1988a.

Geernaert, G. L., Drag coefficient modeling for the near coastal zone, *Dyn. Atmos. Oceans, 11*, 307-322, 1988b.

Geernaert, G. L., and W. J. Plant, *Surface Waves and Fluxes*, Kluwer Acad., Norwell, Mass., 1990.

Geernaert, G. L., K. B. Katsaros, and K. Richter, Variation of the drag coefficient and its dependence on sea state, *J. Geophys. Res., 91*, 7667-7679, 1986.

Geernaert, G. L., S. E. Larsen, and F. Hansen, Measurements of the wind stress, heat flux, and turbulence intensity during storm conditions over the North Sea, *J. Geophys. Res., 92*, 13,127-13,139, 1987.

Geernaert, G. L., F. Hansen, M. Courtney, and T. Herbers, Directional attributes of the ocean surface wind stress vector, *J. Geophys. Res., 98*, 16,571-16,582, 1993.

Hasselmann, K., et al., Measurements of wind-wave growth and swell decay during the Joint North Sea Wave Project (JONSWAP), *Dtsch. Hydrogr. Z., Suppl., Ser A 8(12)*, 1973.

Horst, T. W., and J. C. Weil, How far is far enough?: The fetch requirements for micrometeorological measurement of surface fluxes, *J. Atmos. Oceanic Technol., 11*, 1018-1025, 1994.

Hwang, P. A., and O. H. Shemdin, The dependence of sea surface slope on atmospheric stability and swell conditions, *J. Geophys. Res., 93*, 13,903-13,912, 1988.

Keller, W. C., W. J. Plant, and D. E. Weissman, The dependence of the X band microwave sea return on atmospheric stability and sea state, *J. Geophys. Res., 90*, 1019-1029, 1985.

Kitaigorodskii, S. A., *The Physics of Air-Sea Interaction*, translated from Russian, 273 pp., Isr. Program for Sci. Transl., Jerusalem, 1973.

Kraus, E. B., and J. A. Businger, *Atmosphere-Ocean Interaction*, Oxford Univ. Press, New York, 1994.

Mahrt, L., The coastal zone, in *Air-Sea Exchange: Physics, Chemistry, and Dynamics*, edited by G. L. Geernaert, Kluwer Acad., Norwell, Mass., 1999.

Mahrt, L., D. Vickers, J. Howell, J. Højstrup, J. M. Wilczak, J. Edson, and J. Hare, Sea surface drag coefficient in the Risø Air Sea Experiment, *J. Geophys. Res., 101*, 14,327-14,335, 1996.

Mahrt, L., D. Vickers, J. Edson, J. Sun, J. Højstrup, J. Hare, and J.M. Wilczak, Heat flux in the coastal zone. *Boundary Layer Meteorol., 86*, 421-446, 1998.

Nordeng, T. E., On the wave age dependent drag coefficient and roughness length at sea, *J. Geophys. Res., 96*, 7167-7174, 1991.

Paulson, C. A., The mathematical representation of wind speed and temperature profiles in the unstable atmospheric surface layer, *J. Appl. Meteorol., 9*, 857-861, 1970.

Plant, W. J., W. C. Keller, V. Hesany, K. Hays, K. W. Hoppel, and T. V. Blanc, Measurements of the marine boundary layer from an airship, *J. Atmos. Oceanic Technol., 15*, 1433-1458, 1998.

Rieder, K. F., J. A. Smith, and R. A. Weller, Observed directional characteristics of the wind, wind stress, and surface waves on the open ocean, *J. Geophys. Res., 99*, 22,589-22,596, 1994.

Smedman, Ann-Sofi, H. Bergström, and U. Högström, Spectra, variances and length scales in a marine stable boundary layer dominated by a low level jet, *Boundary Layer Meteorol., 76*, 211-232, 1995.

Smith, S. D., Wind stress and heat flux over the ocean in gale force winds, *J. Phys. Oceanogr., 10*, 709-726, 1980.

Sun, J., Diurnal variations of thermal roughness height over a grassland, *Boundary Layer Meteorol., 92*, 407-427, 1999.

Torrence, C., and G. P. Compo, A practical guide to wavelet analysis, *Bull. Am. Meteorol. Soc., 79*, 61-78, 1998.

Vandemark, D., J. B. Edson, and B. Chapron, Altimeter estimation of sea surface wind stress for light to moderate winds, *J. Atmos. Oceanic Technol., 14*, 716-722, 1997.

Vandemark, D., T. Crawford, R. Dobosy, T. Elfouhaily, and B. Chapron, Sea surface slope statistics from a low-altitude aircraft, *IEEE Proc. of IGARSS, Hamburg, 1999.*

Vandemark, D., P. D. Mourad, T. L. Crawford, C. A. Vogel, J. Sun, S. A. Bailey, and B. Chapron, Measured changes in ocean surface roughness due to atmospheric boundary layer rolls, *J. Geophys. Res., 106*, 4639-4654, 2001.

Vickers, D., and L. Mahrt, Fetch limited drag coefficients, *Boundary Layer Meteorol., 85*, 53-79, 1997a.

Vickers, D., and L. Mahrt, Quality control and flux sampling problems for tower and aircraft data, *J. Atmos. Oceanic Technol., 14*, 512-526, 1997b.

Vickers, D., and L. Mahrt, Observations of non-dimensional wind shear in the coastal zone, *Q. J. R. Meteorol. Soc., 125*, 2685-2702, 1999.

Vickers, D., and L. Mahrt, J. Sun, and T. Crawford, Structure of off-shore flow, *Mon. Weather Rev.*, in press, 2001.

Weller, R. A., M. A. Donelan, M. G. Briscoe, and N. E. Huang, Riding the crest: A tale of two wave experiments, *Bull. Am. Meteorol. Soc., 14*, 835-848, 1991.

Wu, J., Sea-surface slope and equilibrium wind-wave spectra, *Phys. Fluids, 15*, 741-747, 1972.

Wu, J., Effects of atmospheric stability on ocean ripples: A comparison between optical and microwave measurements, *J. Geophys. Res., 96*, 7265-7269, 1991.

T. Crawford, NOAA/FRD, 1750 Foote Drive, Idaho Falls, ID 83402. (tim.crawford@noaa.gov)

L. Mahrt and D. Vickers, College of Oceanic and Atmospheric Sciences, Oregon State University, Corvallis, OR 97331. (mahrt@oce.orst.edu; vickers@oce.orst.edu)

J. Sun, National Center for Atmospheric Research, P.O. Box 3000, Boulder, CO 80307-3000. (jsun@ucar.edu)

D. Vandemark, NASA/GSFC, Code 972, Wallops Island, VA 23337. (vandemark@gsfc.nasa.gov)

C. Vogel, NOAA/ATDD, P.O. Box 2456, Oak Ridge, TN 37831-2456. (vogel@atdd.noaa.gov)

(Received March 2, 2000; revised September 27, 2000; accepted October 5, 2000.)